THE ASTROPHYSICAL JOURNAL SUPPLEMENT SERIES, 110:287–297, 1997 June

PHYSICAL CONDITIONS OF THE CORONAL LINE REGION IN SEYFERT GALAXIES

JASON W. FERGUSON, KIRK T. KORISTA, AND GARY J. FERLAND
Department of Physics and Astronomy, University of Kentucky, 177 Chemistry/Physics Building, Lexington, KY 40506-0055
Received 1996 August 1; accepted 1997 January 10

ABSTRACT

The launch of the *Infrared Space Observatory* and new atomic data have opened a window for the study of high-ionization gas in active galactic nuclei (AGNs). We present the results of a large number of photoionization simulations of the "coronal line" region in AGNs, employing new atomic data from the Opacity and Iron Projects. Our grid of line emission spans 8 orders of magnitude in gas density and 14 orders of magnitude in ionizing flux in an effort to identify the optimal conditions in which these lines form. We show that coronal lines form at distances from just outside the broad-line region to $\sim 400 L_{43.5}^{1/2}$ pc, in gas with ionization parameter $-2.0 \lesssim \log U(H) \lesssim 0.75$, corresponding to gas densities of 10^2–$10^{8.5}$ cm^{-3}, with electron temperatures $\sim$12,000–150,000 K. A large range of distances from the central source implies significant line width variation among the coronal lines. We identify several line ratios that could be used to measure relative abundances, and we use these to show that the coronal line gas is likely to be dust free.

Subject headings: galaxies: Seyfert — infrared: galaxies — line: formation

1. INTRODUCTION

Given their high-ionization potentials ($\chi > 100$ eV), the presence of highly ionized optical forbidden lines, such as [Fe VII] λ6087, [Fe X] λ6375, [Fe XI] λ7892, and [Fe XIV] λ5303, in the spectra of Seyfert galaxies points to very energetic processes at work in these active galactic nuclei (AGNs) (Oke & Sargent 1968; Souffrin 1968; Grandi 1978; Penston et al. 1984). If mechanically shocked and collisionally ionized, this gas is as hot as our Sun's corona, 10^6 K, thus the origin of their name, "coronal lines." On the other hand, if photoionized by the hard ionizing continuum of the AGN, the coronal emission line gas is expected to be only a few to several tens of thousands of degrees (Nussbaumer & Osterbrock 1970; Grandi 1978; Korista & Ferland 1989; Oliva et al. 1994; Pier & Voit 1995; Oliva 1996).

Recent observations of the optical coronal line profiles show that they have FWHM broader than those of lower ionization forbidden lines, such as [O III] λ5007 (De Robertis & Osterbrock 1984, 1986; Appenzeller & Östreicher 1988; Appenzeller & Wagner 1991; Veilleux 1991). This, and the fact that the coronal emission line critical densities are also larger (10^7–10^{10} cm^{-3}), has led to speculation that these lines form in a region intermediate between the classical narrow-line region and the broad-line region.

New ground-based infrared observations have focused on the strongest lines visible through infrared windows in the Earth's atmosphere, namely, [Mg VIII] 3.03 μm, [Si VI] 1.96 μm, [Si VII] 2.47 μm, [Si IX] 3.92 μm, [Si X] 1.43 μm, [S IX] 1.25 μm, and [Ca VIII] 2.32 μm (see Oliva & Moorwood 1990; Spinoglio & Malkan 1992; Voit 1992; Oliva et al. 1994; Giannuzzo, Rieke, & Rieke 1995; Marconi et al. 1996; Thompson 1996). However, the new *Infrared Space Observatory* (*ISO*) is now producing high-quality infrared spectra of Seyfert galaxies over a broad wavelength range (Kessler 1996; Moorwood et al. 1996).

With the advent of modern infrared spectroscopy and new atomic data computations from the Opacity Project (Seaton et al. 1992) and the Iron Project (Hummer et al. 1993), the opportunity to understand the origin and nature of this high-ionization emission is upon us. To this end, we present the results of a large grid of photoionization calculations in which we illustrate graphically those parameters, the radius from the central ionizing source and gas density, that produce 24 coronal lines most efficiently. These will be important tools for the quantitative spectroscopist interested in understanding the physical conditions in which coronal lines arise.

2. MODEL CALCULATIONS

2.1. *New Atomic Database for the Coronal Lines*

Recent years have seen the emergence of accurate computations of collision strengths, led by the efforts of the Iron Project. We present model calculations of coronal emission lines using the data from Lennon & Burke (1994; [Ne V], [Mg VII], [Al VIII], [Si IX], [S XI]), Zhang, Graziani, & Pradhan (1994; [Ne VI], [Mg VIII], [Si X]), Saraph & Tully (1994; [Al V], [Si VI], [S VIII], [Ar X]), Butler & Zeippen (1994; [Mg V], [Al VI], [Si VII], [S IX], [Ar XI]), Pelan & Berrington (1995; [Fe X]), and Storey, Mason, & Saraph (1996; [Fe XIV]). We discuss possible problems with the new iron collision strengths in § 3.3. Most of the Einstein transition probabilities were taken from Kaufman & Sugar (1986), and photoionization cross sections are from Verner et al. (1996), many of which are fits to cross sections generated by the Opacity Project. The cross sections of many of these ions have changed significantly from those used by Korista & Ferland (1989). The other major uncertainty in the results presented here, other than the iron coronal line collision strengths, is the ionization balance of the third and fourth row elements (most of the ions presented here), due to uncertainties in the low-temperature dielectronic recombination rates for these elements (see Nussbaumer & Storey 1984 and Ali et al. 1991).

2.2. *Assumptions*

We assume that the origin of the coronal line emission is from gas photoionized primarily by the central AGN, although in some cases shocks from strong radio jets may be important (Tadhunter et al. 1988; Morse, Raymond, & Wilson 1996). The origin of the gas is presently unknown

but may be related to galactic H II regions and molecular clouds (Korista & Ferland 1989; Oliva et al. 1994; Pier & Voit 1995). We have used the spectral synthesis code CLOUDY (version 90.02; Ferland 1996) to calculate the emission from plane-parallel, constant hydrogen density clouds ionized by a continuum similar to a typical Seyfert galaxy with $L_{\rm ion} = 10^{43.5}$. The shape of the ionizing continuum was chosen to be a combination of a UV bump of the form $f_\nu \propto \nu^{-0.3} \exp(-h\nu/kT_{\rm cut})$ and an X-ray power law of the form $f_\nu \propto \nu^{-1.0}$ spanning 13.6 eV–100 keV. The UV-bump cutoff temperature, $T_{\rm cut}$, was chosen such that the UV bump peaked (in νF_ν) at 48 eV. The UV and X-ray components were combined with a typical Seyfert UV–to–X-ray spectral slope, $\alpha_{\rm ox} = -1.2$.

CLOUDY now considers the ionization balance of the first 30 elements; we assume solar abundances from Grevesse & Anders (1989) and Grevesse & Noels (1993): H, 1.00E+00; He, 1.00E−01; Li, 2.04E−09; Be, 2.63E−11; B, 7.59E−10; C, 3.55E−04; N, 9.33E−05; O, 7.41E−04; F, 3.02E−08; Ne, 1.17E−04; Na, 2.06E−06; Mg, 3.80E−05; Al, 2.95E−06; Si, 3.55E−05; P, 3.73E−07; S, 1.62E−05; Cl, 1.88E−07; Ar, 3.98E−06; K, 1.35E−07; Ca, 2.29E−06; Sc, 1.58E−09; Ti, 1.10E−07; V, 1.05E−08; Cr, 4.84E−07; Mn, 3.42E−07; Fe, 3.24E−05; Co, 8.32E−08; Ni, 1.76E−06; Cu, 1.87E−08; Zn, 4.52E−08.

While grains are present in at least the partially shielded portions of narrow-line region clouds (Ferland 1993), we will show (§ 2.4) that they are likely absent in the coronal line–emitting gas (see also Korista & Ferland 1989 and Oliva et al. 1994).

The ionization/thermal equilibrium and radiative transfer calculations for a single cloud proceeded until one of the following conditions was met: (1) the electron temperature dropped below 3000 K, (2) the thickness of the cloud exceeded 10% of its distance from the central continuum source (in keeping with plane-parallel clouds), or (3) the total hydrogen column density exceeded 10^{24} cm^{-2}. In practice, the third condition had little impact on the coronal emission lines. The plane-parallel condition was invoked to avoid clouds whose dimensions rival their distances from the central source, thus avoiding a significant covering fraction by a single cloud. The largest cloud of the grid presented below is one with a thickness of $\sim$16 pc, consistent with the size of large molecular clouds. We will comment further on the effects of these stopping criteria in a later section.

Finally, we assume that each cloud sees the full continuum with no obscuration. At large enough distances, the clouds or the diffuse interstellar medium (ISM) may attenuate the ionizing spectrum significantly.

2.3. *Reprocessing Efficiency*

Given the assumptions above, the emission from 1881 individual clouds has been computed as a function of the cloud distance from the ionizing source, log R (cm), and the hydrogen number density of the cloud, log $n(H)$ (cm^{-3}). We attempted to span all expected phase space in the cloud distance–gas density plane necessary to emit the coronal lines. For the assumed source luminosity, the cloud distances spanned approximately 0.5 light-days to 3 kpc; the gas density spanned 8 orders of magnitude, 10^2–10^{10} cm^{-3}. Coronal line–emitting gas with significantly lower densities will have vanishingly smaller surface brightnesses and thus will not be considered here. The cloud distances will scale with luminosity as $L_{43.5}^{1/2}$, where $L_{43.5}$ is the ionizing luminosity in units of $10^{43.5}$ ergs s^{-1}. Note that this scaling with observed luminosity assumes that the continuum is emitted isotropically, which may not be the case in nature. Recent observations have shown emission-line "cones" (Evans et al. 1991; Tsvetanov & Walsh 1992; Wilson et al. 1993; Macchetto et al. 1994; Arribas, Mediavilla, & García-Lorenzo 1996) and UV photon deficits (Binette, Fosbury, & Parker 1993; Morse et al. 1996). This "beaming" of the incident continuum, which the clouds see and we may not, will change the effective luminosity incident on the clouds and adjust the distances presented below.

Contour plots of emission-line equivalent width, referred to the incident continuum at 4860 Å, as a function of log R and log $n(H)$ for 24 high-ionization forbidden lines are shown in Figures 1, 2, 3, and 4. This equivalent width assumes 100% source coverage by the emitting clouds. We show those lines that are expected to be either strong and/or observationally important. The emission-line equivalent width distributions are plotted in order of increasing atomic number, then increasing ionization stage for each element, and indicate the efficiency of continuum reprocessing.

For each emission line in Figures 1–4, a ridge of near-maximum equivalent width runs diagonally across the distance–gas density plane, roughly parallel to lines of constant ionization parameter. The ionization parameter, $U(H)$, is defined as the ratio of ionizing photon density to hydrogen density, $U(H) \equiv \Phi(H)/n(H)c$, where $\Phi(H)$ is the flux of ionizing photons and c is the speed of light. This parameter increases from top right to bottom left in these diagrams, and log $U(H) = -4.0$ is plotted as a dashed line for each emission line as a reference. This ridge of near-maximum equivalent width coincides with a small range in optimal ionization parameter. For larger (smaller) ionization parameters, the gas is over(under)ionized, and the line is not emitted efficiently. This explains the sudden drops in the emission-line equivalent widths on either side of their ridges. The asymmetric drop of emission on either side of the ridges is explained by the differing physical conditions of the gas on either side of the ridges and by our assumption of plane-parallel clouds (§ 2.2). The latter has the effect of truncating the emission of some of the "lower ionization" coronal lines, such as [Ne V], at high-ionization parameter where they would otherwise form on the back sides of the clouds. In the absence of this truncation, the ridges of optimal emission would broaden slightly in the direction of higher ionization parameter. The effect on the higher ionization coronal lines is minimal since these lines generally form in a thin zone on the side of the cloud facing the ionizing source.

Moving *along* the ridge to increasing gas densities, at near-constant ionization parameter, the forbidden lines become collisionally de-excited, and the line equivalent width falls off. Let us compare, for example, in Figures 1*a* and 1*b*, the near-UV and infrared transitions of [Ne V]. Moving along the ridge at constant ionization parameter to smaller gas densities, the equivalent widths of some lines also diminish as other lines of similar ionization, but lower critical density, become important coolants. These contour plots represent "visibility functions" for the coronal lines.

In Table 1, we give the ionization parameter at the peak equivalent width (col. [3]) and the range in log $n(H)$ for the top contour (col. [4]) of each line considered in Figures 1–4. Together, these parameters describe the optimal conditions

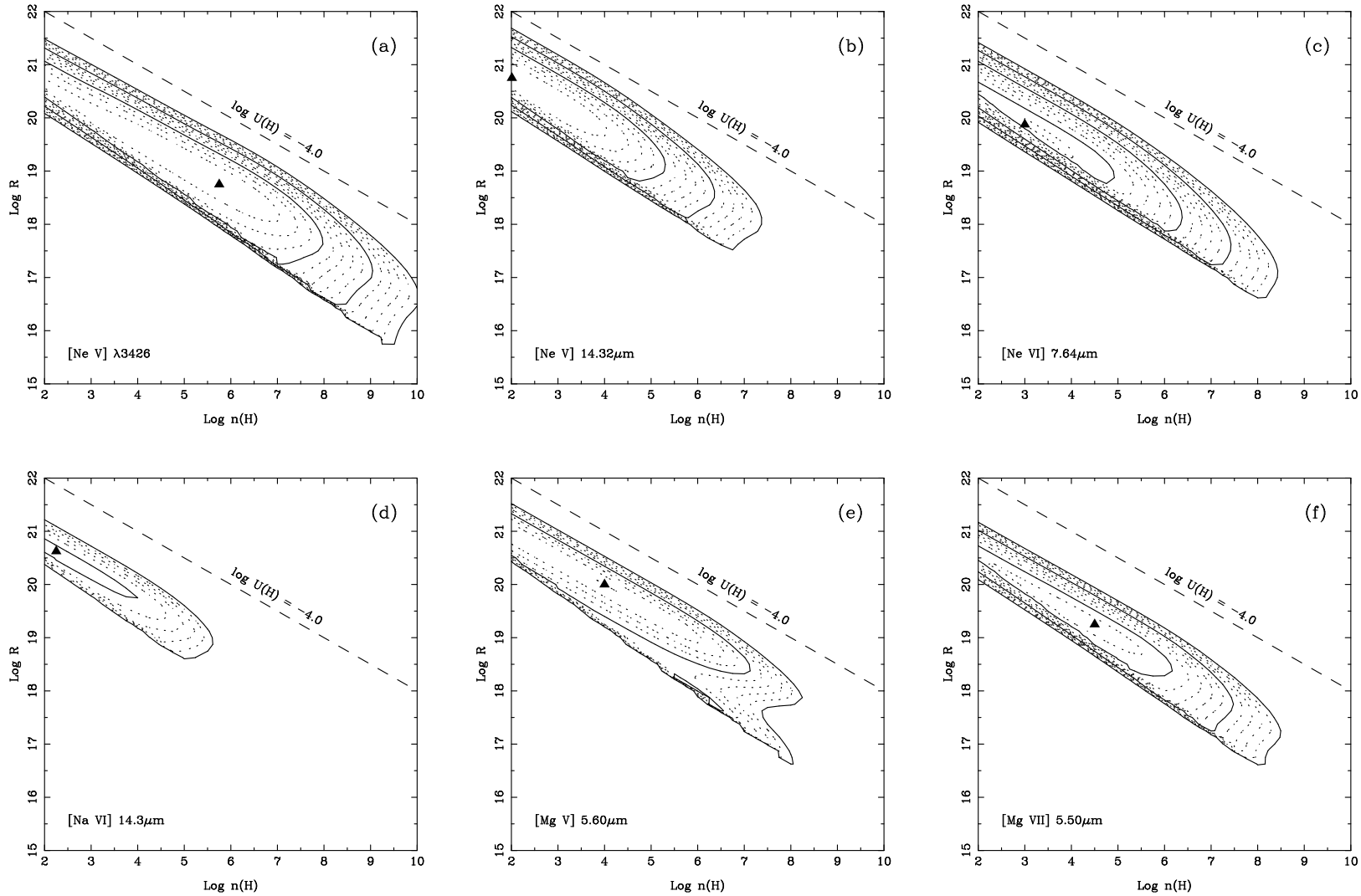

FIG. 1.—Contours of constant logarithmic line equivalent widths as a function of log R and log $n(H)$ for the ions indicated, referenced to the incident continuum at 4860 Å. The thick lines represent 1 dex, and the dotted lines are 0.2 dex steps. The triangle is the peak of the equivalent width distribution, and the contours decrease downward to the outer value of 1 Å. The reader will sometimes find it convenient to view the contour plots *along* the ridge at large inclination angle to the sheet of paper.

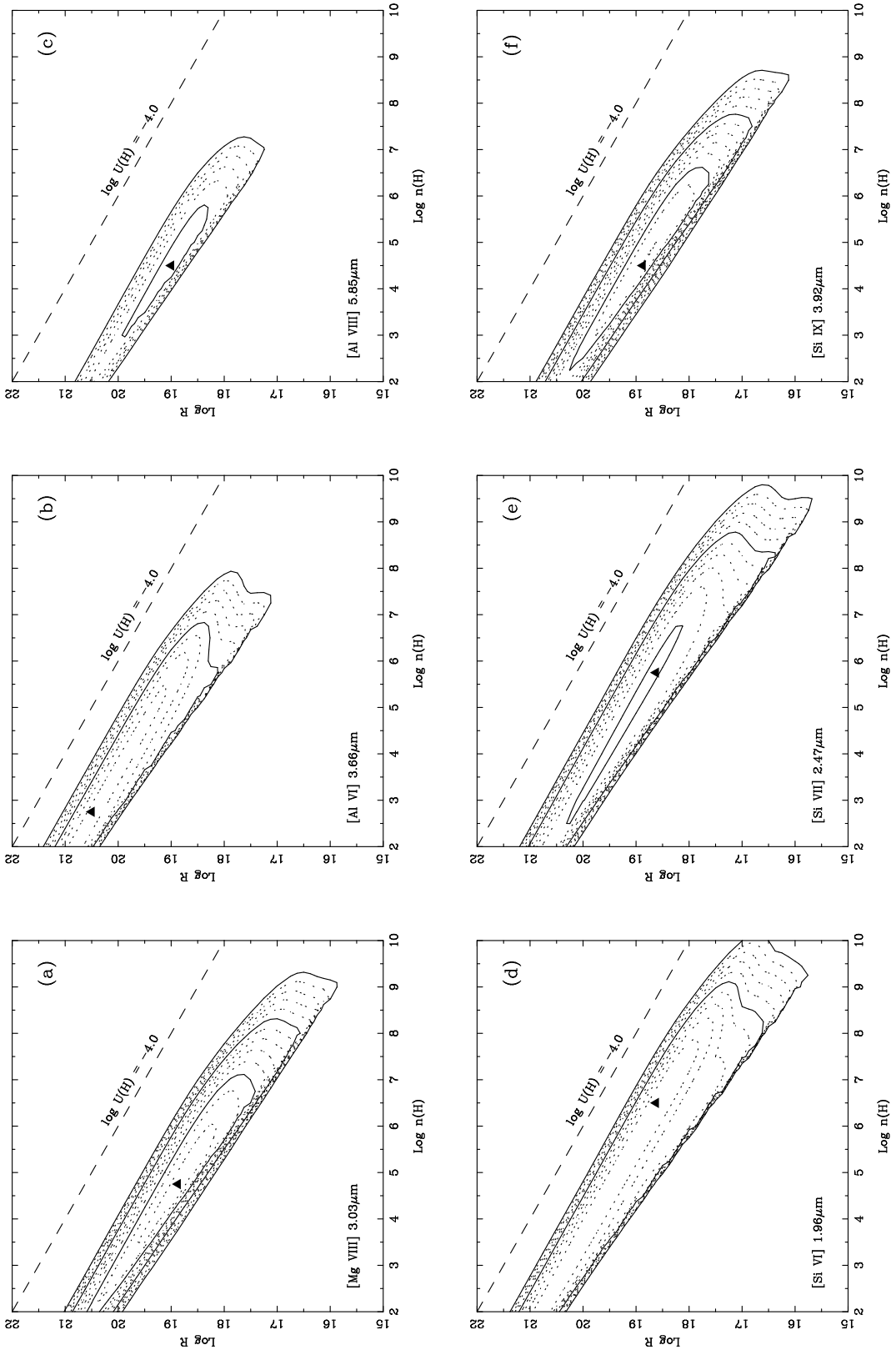

FIG. 2.—Same as Fig. 1, but for the ions indicated

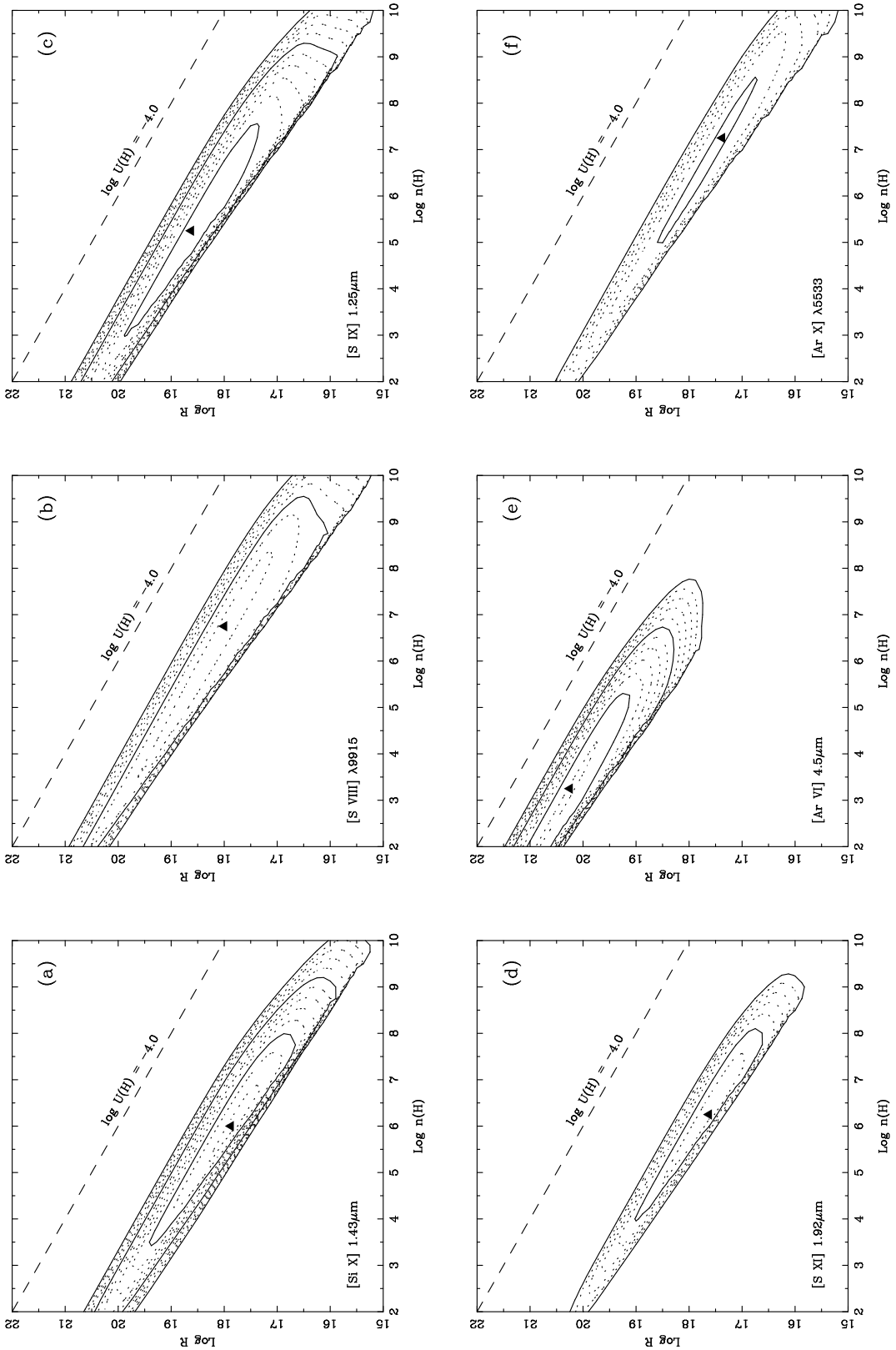

FIG. 3.—Same as Fig. 1, but for the ions indicated

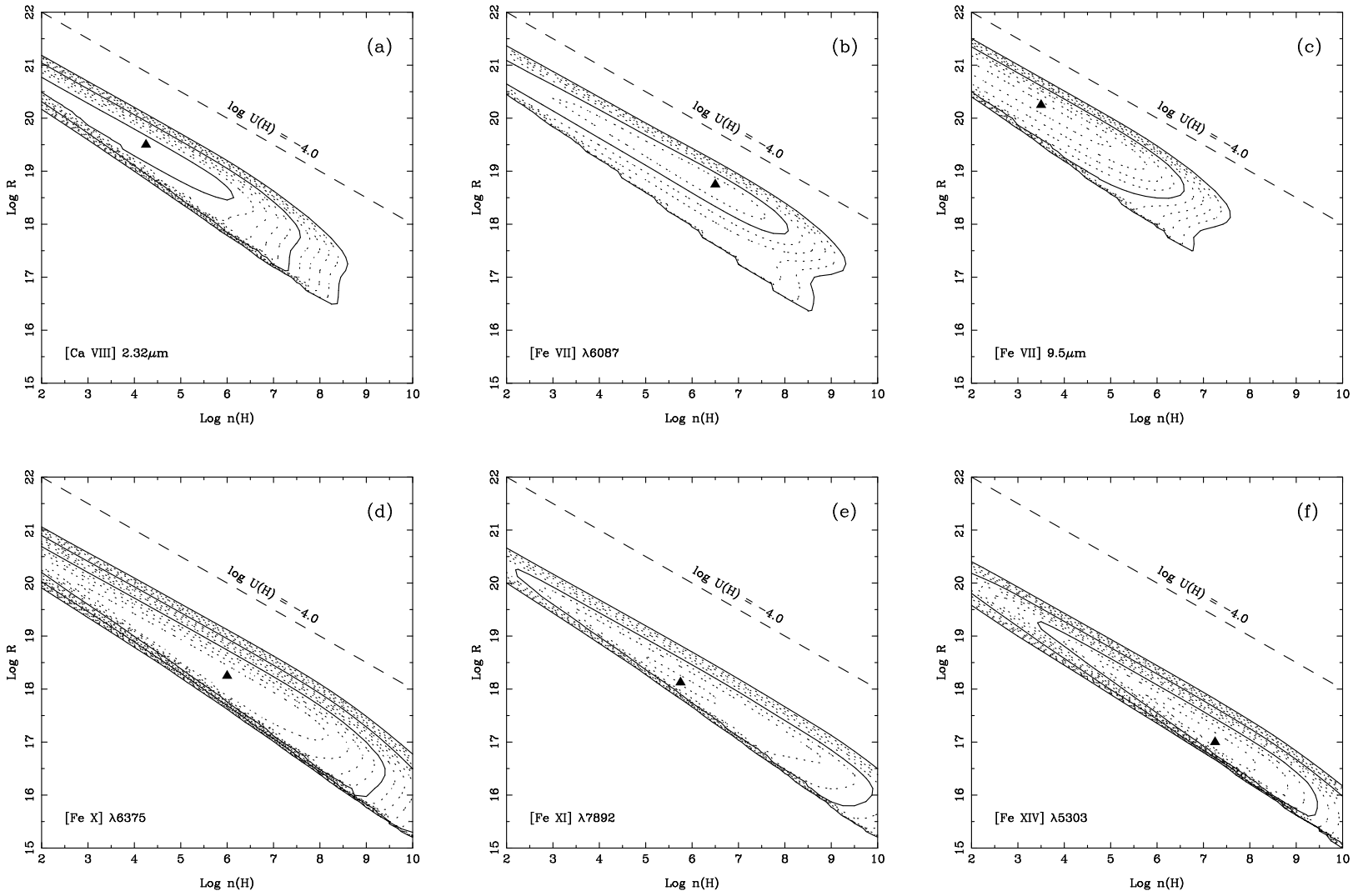

FIG. 4.—Same as Fig. 1, but for the ions indicated

TABLE 1

CORONAL LINE PHYSICAL CONDITIONS

Ion (1)	λ[a] (2)	log $U(H)$[b] (3)	Range log $n(H)$[c] (4)	Range log R[d] (5)	Peak log T_e[e] (6)	$W_{\lambda 4860}^{max}$[f] (7)
[N V]	λ3426	−1.25	*L*–7.0	18.1–20.6	4.3	621
	14.32 μm	−1.5	*L*–4.0	19.8–20.8	4.2	930
[Ne VI]	7.64 μm	−0.75	3.0–4.0	19.4–19.9	4.4	1728
[Na VI]	14.3 μm	−1.5	*L*–4.0	19.8–20.8	4.2	11.6
[Mg V]	5.60 μm	−2.0	*L*–6.0	19.0–21.0	4.2	63.2
[Mg VII]	5.50 μm	−1.0	2.5–5.5	18.8–20.3	4.3	184
[Mg VIII]	3.03 μm	−0.5	3.5–6.0	18.3–19.5	4.4	298
[Al VI]	3.66 μm	−1.75	*L*–5.5	19.1–20.9	4.2	48.3
[Al VIII]	5.85 μm	−0.5	2.75–5.75	18.4–19.9	4.4	12.8
[Si VI]	1.96 μm	−1.75	*L*–7.75	18.0–20.9	4.2	93.1
[Si VII]	2.47 μm	−1.0	2.25–6.75	18.1–20.4	4.3	110
[Si IX]	3.92 μm	−0.25	3.0–6.25	18.0–19.6	4.5	256
[Si X]	1.43 μm	0.25	5.25–7.0	17.4–18.3	4.8	284
[Si VIII]	λ9915	−0.75	3.5–8.25	17.3–19.6	4.5	28.5
[S IX]	1.25 μm	−0.5	3.0–7.75	17.4–19.8	5.0	143
[S XI]	1.92 μm	0.5	4.75–7.5	17.0–18.4	5.1	20.2
[Ar VI]	4.53 μm	−1.75	*L*–4.25	19.8–20.9	4.2	166
[Ar X]	λ5533	0.0	5.0–8.5	16.8–18.5	4.6	11.6
[Ca VIII]	2.32 μm	−1.25	*L*–6.25	18.5–20.6	4.3	152
[Fe VII]	λ6087	−2.0	3.0–7.5	18.3–20.5	4.2	21.2
	9.51 μm	−2.0	*L*–5.0	19.5–21.0	4.2	71.7
[Fe X]	λ6375	−0.5	3.0–8.25	17.1–19.8	4.6	968
[Fe XI]	λ7892	0.0	5.0–6.5	17.8–18.5	4.6	41.2
[Fe XIV]	λ5303	0.75	5.75–8.0	16.6–17.8	5.2	468

[a] Wavelengths in angstrom units for the optical lines or microns for the IR lines.
[b] Value of the dimensionless ionization parameter at the triangle in Fig. 1.
[c] Minimum and maximum log $n(H)$ (cm^{-3}). Values of *L* indicate that the top ridge extends below the cutoff value of log $n(H) = 2$.
[d] Minimum and maximum log R (cm) corresponding to the maximum and minimum log $n(H)$ for the peak log $U(H)$ in col. (3).
[e] Log electron temperature (K) at front face of the cloud with log $U(H)$ given in col. (3).
[f] Peak $W_{\lambda 4860}$ (Å) of line in Fig. 1 for a cloud-covering factor of 1.

in which these lines form. Note that a range in gas density for a given ionization parameter indicates a range of expected distances from the central source for $L_{ion} = 10^{43.5}$ ergs s^{-1}, given in column (5) of Table 1. We emphasize that these distance ranges are not *necessarily* those for which the coronal lines should be most luminous in Seyfert galaxies. For example, we do not expect a substantial contribution of coronal line emission from the broad emission line region. Rather, column (5) is meant to illustrate the relative differences in the coronal line formation distances. In column (6), we give the log T_e (K) of the front face of the cloud whose ionization parameter is given in column (3). This temperature is representative of that in which the line in column (1) is emitted. Column (7) lists the peak equivalent width of each line, as indicated in Figure 1. Since this equivalent width is referenced to the same point in the incident continuum, a comparison should indicate grossly the expected relative strengths of these lines, although this is not meant to represent a predicted coronal emission line spectrum that is outside the scope of the present paper.

2.4. *Dust in the Coronal Line Gas?*

Pier & Voit (1995) hypothesized that the coronal line emission comes from a thin, highly ionized "skin" just above the surface of the "obscuring" molecular torus that is undergoing evaporation from an X-ray–heated wind generated by the central continuum source. In this model, the grains are not destroyed until they are sputtered in the 10^6 K wind, with some destruction possible in the coronal line–emitting gas just below the wind. However, their predicted coronal line spectrum assumed solar abundances and did not take into account gas-phase depletions onto grains (Pier 1995). In this section, we demonstrate the full effects of the presence of grains in a more general coronal line–emitting environment.

There are three major effects of dust on line formation: (1) the emission lines weaken because of the absorption of the incident continuum by dust at large $U(H)$, (2) the grains photoelectrically heat the gas, and (3) some of the gas-phase elements are depleted. The destruction of the coronal line photons by grains is included but not important, since the line and IR continuum optical depths are small in comparison with the resonance lines that are readily destroyed by grains. We include dust of the type found in the Orion Nebula (Baldwin et al. 1991) in grid calculations at radii consistent with the sublimation temperatures of the silicate and graphite grains discussed by Laor & Draine (1993) and Netzer & Laor (1993). In particular, inside the graphite grain boundary, the gas had solar abundances, and no grains were present. The Orion-type graphite grains were turned on at a radius of $10^{16.9}$ cm [where T_{dust}(graphite) $\approx$ 1750 K], and the carbon abundance was set to the value given below. The Orion-type silicate grains were turned on at a radius of $10^{17.6}$ cm [where T_{dust}(silicate) $\approx$ 1400 K], and the gas abundances of the important elements then took on those of the ionized gas in the Orion Nebula (see Baldwin et al. 1996): H, 1.00E+00; He, 9.50E−02; C, 3.00E−04; N, 7.00E−05; O, 4.00E−04; Ne, 6.00E−05; Na, 3.00E−07; Mg, 3.00E−06; Al, 2.00E−07; Si, 4.00E−06; S, 1.00E−05; Cl, 1.00E−07; Ar, 3.00E−06; Ca, 2.00E−08; Fe, 3.00E−06; Ni, 1.00E−07.

These abundances are based upon the results of several

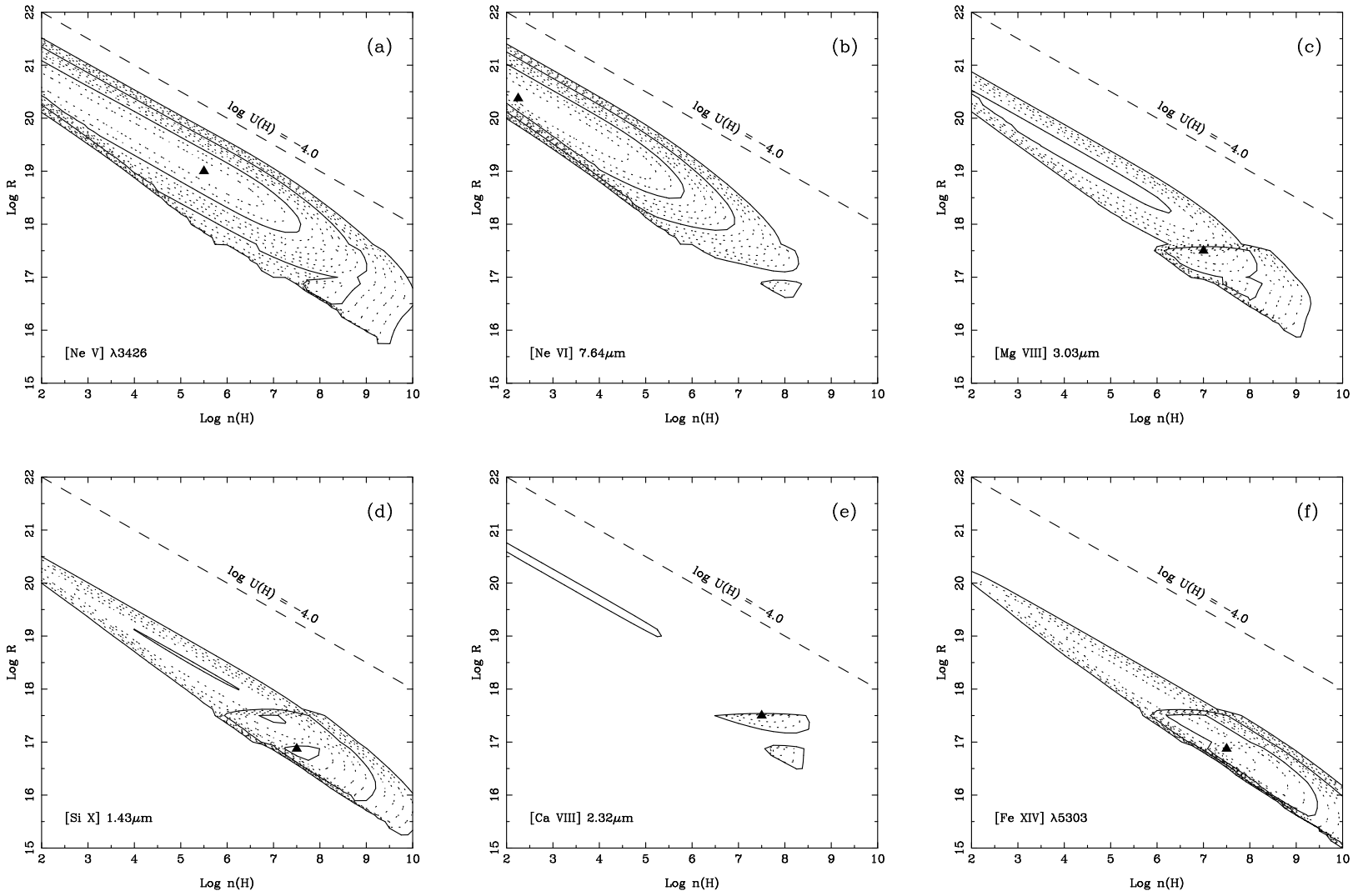

FIG. 5.—Same as Fig. 1, but for the ions indicated, including dust as described in § 2.4

recent studies of the Orion Nebula (Baldwin et al. 1991; Rubin et al. 1991; Rubin, Dufour, & Walter 1992a; Rubin et al. 1992b; Osterbrock, Tran, & Veilleux 1992). Note that while nitrogen and neon are not expected to be depleted onto grains, the current best estimates of their gas-phase abundances are found to be 75% and 50% of their solar values relative to hydrogen, respectively. O/H and C/H are also depressed, their abundances being 54% and 85% solar, respectively. How much of these differences from solar are due to depletions onto grains, or due to intrinsic abundance differences, is unknown and is an area of active research (e.g., Snow & Witt 1996). Since carbon and oxygen do much of the line cooling, some differences in the cloud thermal structure and emission will result, independent of the effects of the grains themselves. A full treatment of the dust physics was included in the simulations (see Baldwin et al. 1991).

In Figure 5, we show the equivalent width contours of six coronal lines formed in the presence of dust, as described above. These lines should be compared with their solar abundance, dust-free gas counterparts in Figures 1–4. A comparison of Figure 5*f* with Figure 4*f* ([Fe XIV] λ5303) illustrates most dramatically the effects on the line emission. At radii smaller than $10^{16.9}$ cm, grains are not present, and the contours shown in Figure 5*f* are exactly those shown in Figure 4*f*. For radii just outside this graphite grain sublimation boundary, iron is not depleted, but a significant decline in the line equivalent width (factor of $\sim$6) occurs because of the first effect mentioned above. This line's equivalent width again falls rapidly just beyond the silicate grain sublimation radius (another factor of $\sim$25). At these larger radii, many of the elements, including iron, are depleted onto grains. Some of the more refractory elements and their Orion depletion factors are Mg(12), Si(12), Ca(115), and Fe(11). Note that these depletions are less severe than in the local ISM and could, in part, represent grain destruction in the ionized gas (Rubin et al. 1992a, 1992b). Mainly because of its extreme depletion in a dusty environment, the emission lines of Ca are devastated (Fig. 5*e*). The peak equivalent width contours of [Mg VIII] 3.03 μm, [Si X] 1.43 μm, and [Ca VIII] 2.32 μm in Figure 5 have smaller values and have moved to smaller radii along their ridges, where the effects of grains are smaller or absent. The effects of the presence of grains on the emission of [Ne V] λ3426 and [Ne VI] 7.64 μm are more subtle. Neon, a noble gas, is not depleted, and these lines are emitted almost entirely outside the grain sublimation radii. These lines suffered declines in their peak equivalent widths of factors of 2 and 3, respectively, and their ridges shifted to lower ionization parameters where the grain/gas opacity ratio is smaller. This effect is not as important for these two lines, compared with the others in Figure 5, since they form at smaller ionization parameters.

Figures 1–5 and column (5) of Table 1 show that the lower ionization coronal lines form in regions outside the dust sublimation radii, while the higher ionization coronal lines form in regions that straddle these radii. Given the severe reduction in many of the coronal line intensities in a dusty environment, the observed strengths of the coronal emission lines indicate that they are formed in dust-free, or nearly so, gas. The observations in several Seyfert galaxies of significant [Ca VIII] 2.32 μm emission relative to [Ne V] λ3426 and [Si VII] 2.47 μm, all formed mainly outside the sublimation radii (Oliva et al. 1994; Marconi et al. 1996), would, by itself, seem to exclude the possibility of the existence of dust within the coronal line gas. We elaborate further on this.

3. DISCUSSION

3.1. *Coronal Line Formation in Photoionized Gas*

The coronal lines shown in Figure 1 form in gas that has typical ionization parameters $-2.0 \lesssim \log U(H) \lesssim 0.75$, gas densities $2.0 \lesssim \log n(H) \lesssim 8.5$ (cm^{-3}), and temperatures $\sim$20,000–150,000 K. This corresponds to distances from the ionizing source of approximately the broad-line region to 400 pc ($L_{43.5}^{1/2}$). This upper limit on the distance could be larger if lower density gas is present, but this gas would have a smaller surface brightness. It is interesting to note that the lower ionization coronal lines, [Ne V]–[Si VII], and also [Ca VIII] and [Fe VII], form most efficiently in gas that is roughly $\sim$10 pc and beyond, and thus their emission may be extended in nearby Seyfert galaxies (Korista & Ferland 1989). The rest of the lines in Table 1 form optimally in gas less than 10 pc from the ionizing source. Looking at Table 1, we expect that [Fe VII] λ6087 and [Fe XIV] λ5303 form in completely different gas. For comparison, [O III] λ5007 is expected to form in gas at distances of several parsecs to $\sim$1 kpc.

If there is a relatively simple relation between the cloud distance and its velocity, then one might expect to find observationally a relationship between the width of the line and its ionization potential and/or critical density; the latter two are related. Such relationships have been observed among the optical forbidden lines (e.g., Filippenko & Halpern 1984; De Robertis & Osterbrock 1984, 1986). Based on Figures 1*a* and 1*b*, and columns (3)–(5) in Table 1, one might expect that the infrared [Ne V] 14.32, 24.3 μm lines would be emitted primarily in gas of very different properties than that of the [Ne V] $\lambda\lambda$3426, 3346 lines, *even though they arise from the same ion.* The near-UV line profiles are likely to be significantly broader than their infrared counterparts. To our knowledge, the infrared lines of [Ne V] have not been reported for Seyfert galaxies but should be observed with *ISO*.

The equivalent widths of the coronal lines should serve as an effective Zanstra temperature (Zanstra 1931; Osterbrock 1989) of the relevant ionizing continuum ($\sim$0.1–0.5 keV). In § 2.2, we assumed a fairly hard continuum incident on the coronal line clouds. Decreasing the coronal ionizing photon flux, Φ(0.1–0.5 keV), by a factor of 10 will decrease the equivalent width of the higher ionization lines, such as [Fe X] and [Si X], by factors of 10 and 20, and the lower ionization lines, such as [Ne V], by factors of 2–3. A more subtle effect of the shape of the ionizing spectrum is that the formation distances of especially the highest ionization coronal lines (col. [5] of Table 1) will shift to smaller (larger) values for significantly softer (harder) spectra, because of changes in the thermal/ionization balance in the clouds. In the example of the diminished Φ(0.1–0.5 keV) above, the formation distances in column (5) of Table 1 would be $\sim$2 times smaller for the highest ionization lines (e.g., [Fe X] λ6375 and [Fe XIV] λ5303), while the effects on lines such as [Ne V] and [Fe VII] would be much smaller. Many of the highest ionization lines might be invisible also.

3.2. *Relative Abundance Determinations*

Nussbaumer & Osterbrock (1970) suggested using the [Fe VII] λ6087/[Ne V] λ3426 ratio to measure the Fe/Ne

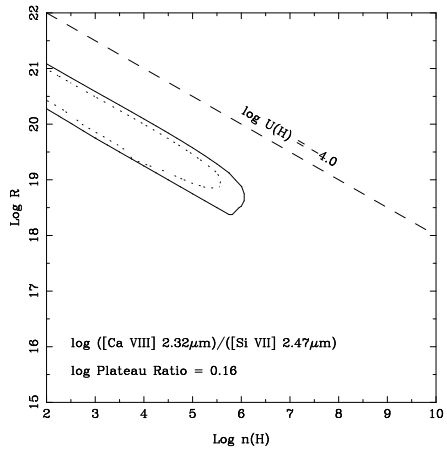

FIG. 6.—Logarithmic contours of the ratio [Ca VIII] 2.32 μm/[Si VII] 2.47 μm. The solid outer contour is a linear ratio of 1, and the dotted lines are 0.1 dex steps. The linear value of the plateau ratio is between 1.4 and 1.5.

abundance. In principle, this would be a good ratio, if the two lines are formed in the same gas, since neon is not expected to be depleted when grains are present. However, a glance at Table 1 and Figures 1*a* and 4*c* shows that these lines generally do not form in the same gas. In this section, we discuss a few coronal line ratios that should prove to be reliable gas abundance indicators.

The ratios of emission lines forming in gas with the same physical conditions, i.e., gas density, temperature, and ionization, will be good relative abundance indicators. Considering Figures 1–4 and Table 1, we have identified several pairs of lines that form in similar physical conditions. Their ridges of peak equivalent widths overlie one another, and their ratio should be nearly flat in the gas density–source distance plane. Figure 6 shows the best example of line ratios that overlap well in the gas density–source distance plane. The ratio [Ca VIII] 2.32 μm/[Si VII] 2.47 μm has a nearly flat plateau, with a linear value between 1.4 and 1.5 for solar gas abundances, although values as small as 1 are possible in some gas where the two lines are strong. Table 2 summarizes the eight most reliable abundance indicators from considering Table 1. Column (2) of the table gives the value of the plateau of the line ratio. For two of the ratios, [Al VI]/[Si VI] and [Ar X]/[Fe XI], the plateau was fairly flat due to the ridges of the individual lines overlapping well, with errors of ∼30%–40%. However, the other ratios were not as well behaved, and the plateau value is only known to a factor of 2, indicating the sensitivity to the line formation conditions. The observed line ratios, if any, are given in column (3) for two Seyfert galaxies, and the solar abundance ratio is given in column (4).

From Table 2, we see that the ratio of [Ca VIII]/[Si VII] is predicted, with solar abundances, to be 2–3 times that of the observed value. Taking the observed ratios at face value, either calcium is underabundant relative to silicon by a factor of 2 or the reverse, silicon is overabundant relative to calcium compared with solar. This is nowhere near the factor of 13 underabundance of calcium relative to silicon in the Orion Nebula (Rubin et al. 1992a, 1992b), or the factor of 225 in the local ISM (Snow & Witt 1996), supporting our earlier statement (§ 2.4) that the coronal line–emitting gas is dust free. This has important implications for the origin of the coronal line gas, as well as the "classical" narrow emission line gas, since there must be some spatial overlap. Are the narrow-line region clouds dusty throughout? Does the sublimation of dust demarcate the narrow and broad emission line regions (Netzer & Laor 1993)? If the source of gas for the coronal lines is dusty (e.g., molecular clouds or torus), how are the grains destroyed in the emitting region? The electron temperatures at the front faces of the coronal line–emitting clouds range from ∼20,000 to 150,000 K, and the destruction of grains due to sputtering is probably unimportant, except on long timescales (Draine & Salpeter 1979). However, some mechanism must be responsible for the destruction of most of the dust in the coronal line–emitting gas.

3.3. *The Iron Conundrum*

Oliva, Pasquali, & Reconditi (1996) highlighted the sensitivity of the collision strengths to the presence and position of resonances in the collisional cross sections. The collision strengths of [Fe X] and [Fe XIV] are now more than an order of magnitude larger than those used in Korista & Ferland (1989), which did not include the effects of resonances (Mason 1975). However, even some of the recent calculations that include resonances differ significantly in their resulting collision strengths. For example, the most

TABLE 2

ABUNDANCE RATIO INDICATORS

Line Ratio[a] (1)	Plateau Ratio[b] (2)	Observed Ratios (3)	Solar Abundance Ratio[c] (4)
[Al VI]/[Si VI]	0.6	...	0.083
[Ar VI]/[Si VI]	1.8–2.2	...	0.11
[Mg VII]/[Si VII].....	1.3–2.5	...	1.07
[Ca VIII]/[S VII]	1.4–1.5	0.81,[d] 0.46[e]	0.065
[Mg VIII]/[S IX]	1.8–3.0	...	2.4
[Al VIII]/[Si IX]	0.07–0.14	...	0.18
[Mg V]/[Fe VII][f].....	0.7–0.9	...	1.17
[Ar X]/[Fe XI]	0.26	...	0.123

[a] Ratio of overlapping lines in Table 1.

[b] Predicted line ratio where nearly constant, or a range is given if the equivalent widths of the two lines do not closely overlap.

[c] Solar abundance ratio of the elements in col. (1).

[d] NGC 1068; Marconi et al. 1996.

[e] Circinus galaxy (A1409 − 65); Oliva et al. 1994.

[f] [Fe VII] 9.51 μm.

recently computed collision strengths of [Fe X] and [Fe XIV] have differed by factors of 3–10 (Mohan, Hibbert, & Kingston 1994; Pelan & Berrington 1995; Dufton & Kingston 1991; Storey et al. 1996). No collision strengths that include resonances have been calculated for [Fe XI], and those that do for [Fe VII] (Keenan & Norrington 1987) may be in doubt. Preliminary analysis (see also col. [7] of Table 1) indicates that if the most recent collision strengths for [Fe X] and [Fe XIV] are correct (Pelan & Berrington 1995; Storey et al. 1996), then the iron abundance would have to be arbitrarily depleted relative to the other elements (e.g., Mg, Si, and Ca) by more than a factor of ~ 10 compared with solar, which does not make sense. The alternative is that the [Fe X] and [Fe XIV] collision strengths are too strong by a similar factor. We hope that these issues will be resolved in the future. The line ratios involving Fe are currently uncertain, but these and the relative abundance ratios should scale roughly with changes in the iron lines' collision strengths.

4. SUMMARY

Using a large number of photoionization simulations, we have illustrated the physical conditions (gas density and distance from the ionizing source) in which the coronal emission lines in Seyfert galaxy spectra form. We find that the observations of significant emission from ions of refractive elements such as calcium and iron likely excludes the presence of dust grains in the coronal line–emitting gas. The lower ionization coronal lines (e.g., [Ne V] and [Fe VII]) are likely to form in lower density gas that should be spatially extended in nearby Seyfert galaxies, whereas the highest ionization lines (e.g., [Si X] and [Fe XIV]) are likely to form in higher density gas in more compact regions. We expect that the coronal line region is up to $\sim 400 L_{43.5}^{1/2}$ pc in size. Spatially resolved spectroscopy of the optical and infrared coronal lines would prove invaluable to our understanding of these high-ionization emission lines.

We thank NASA and NSF for support through NAG-3223 and AST 93-19034, and STScI for GO-06006.02.

REFERENCES

Ali, B., Blum, R. D., Bumgardner, T. E., Cranmer, S. R., Ferland, G. J., Haefner, R. I., & Tiede, G. P. 1991, PASP, 103, 1182
Appenzeller, I., & Östreicher, R. 1988, AJ, 95, 45
Appenzeller, I., & Wagner, S. J. 1991, A&A, 250, 57
Arribas, S., Mediavilla, E., & García-Lorenzo, B. 1996, ApJ, 463, 509
Baldwin, J. A., et al. 1996, ApJ, 468, L115
Baldwin, J. A., Ferland, G. J., Martin, P. G., Corbin, M. R., Cota, S. A., Peterson, B. M., & Slettebak, A. 1991, ApJ, 374, 580
Binette, L., Fosbury, R. A., & Parker, D. 1993, PASP, 105, 1150
Butler, K., & Zeippen, C. J. 1994, A&AS, 108, 1
De Robertis, M. M., & Osterbrock, D. E. 1984, ApJ, 286, 171
———. 1986, ApJ, 301, 727
Draine, B. T., & Salpeter, E. E. 1979, ApJ, 231, 77
Dufton, O. L., & Kingston, A. E. 1991, Phys. Scr., 43, 386
Evans, I. N., Ford, H. C., Kinney, A. L., Antonucci, R. R. J., Armus, L., & Caganoff, S. 1991, ApJ, 369, L27
Ferland, G. J. 1993, in Proc. Madrid Meeting on the Nearest Active Galaxies, ed. J. E. Beckman, H. Netzer, & L. Colina (Madrid: Consejo Superior de Investigaciones Cientificas), 75
———. 1996, HAZY, a Brief Introduction to CLOUDY, Univ. Kentucky Dept. Phys. Astron. Internal Rep.
Filippenko, A. V., & Halpern, J. P. 1984, ApJ, 285, 458
Giannuzzo, E., Rieke, G. H., & Rieke, M. J. 1995, ApJ, 446, L5
Grandi, S. A. 1978, ApJ, 221, 501
Grevesse, N., & Anders, E. 1989, in AIP Conf. Proc. 183, Cosmic Abundances of Matter, ed. C. J. Waddington (New York: AIP), 1
Grevesse, N., & Noels, A. 1993, in Origin and Evolution of the Elements, ed. N. Prantzos, E. Vangioni-Flam, & M. Casse (Cambridge: Cambridge Univ. Press), 15
Hummer, D. G., et al. 1993, A&A, 279, 289
Kaufman, V., & Sugar, J. 1986, J. Phys. Chem. Ref. Data, 15, 321
Keenan, F. P., & Norrington, P. H. 1987, A&A, 181, 370
Kessler, M. F. 1996, BAAS, 28, 901
Korista, K. T., & Ferland, G. J. 1989, ApJ, 343, 678
Laor, A., & Draine, B. T. 1993, ApJ, 402, 441
Lennon, D. J., & Burke, V. M. 1994, A&AS, 103, 273
Macchetto, F., Capetti, W. B., Sparks, W. B., Axon, D. J., & Boksenberg, A. 1994, ApJ, 435, L15
Marconi, A., van der Werf, P. P., Moorwood, A. F. M., & Oliva, E. 1996, A&A, 308, 1
Mason, H. E. 1975, MNRAS, 170, 651
Mohan, M., Hibbert, A., & Kingston, A. E. 1994, ApJ, 434, 389
Moorwood, A. F. M., Lutz, D., Oliva, E., Marconi, A., Netzer, H., Genzel, R., Sturm, E., & de Graauw, Th. 1996, A&A, in press
Morse, J. A., Raymond, J. C., & Wilson, A. S. 1996, PASP, 108, 426
Netzer, H., & Laor, A. 1993, ApJ, 404, L51
Nussbaumer, H., & Osterbrock, D. E. 1970, ApJ, 161, 811
Nussbaumer, H., & Storey, P. J. 1984, A&AS, 56, 293
Oke, S., & Sargent, W. 1968, ApJ, 151, 807
Oliva, E. 1996, in IAU Colloq. 159, Emission Lines in Active Galaxies: New Methods and Techniques, ed. B. M. Peterson, F.-Z. Cheng, & A. S. Wilson (San Francisco: ASP), in press
Oliva, E., & Moorwood, A. F. M. 1990, ApJ, 348, L5
Oliva, E., Pasquali, A., & Reconditi, M. 1996, A&A, 305, 210
Oliva, E., Salvati, M., Moorwood, A. F. M., & Marconi, A. 1994, A&A, 288, 457
Osterbrock, D. E. 1989, Astrophysics of Gaseous Nebulae and Active Galactic Nuclei (Mill Valley: University Science Books)
Osterbrock, D. E., Tran, H. D., & Veilleux, S. 1992, ApJ, 389, 305
Pelan, J., & Berrington, K. A. 1995, A&AS, 110, 209
Penston, M. V., et al. 1984, Ann. d'Astrophys., 31, 569
Pier, E. A. 1995, private communication
Pier, E. A., & Voit, G. M. 1995, ApJ, 450, 628
Rubin, R. H., Dufour, R. J., & Walter, D. K. 1992a, ApJ, 413, 242
Rubin, R. H., Erickson, E. F., Hass, M. R., Colgan, S. W. J., Simpson, J. P., & Dufour, R. J. 1992b, in IAU Symp. 150, The Astrochemistry of Cosmic Phenomena, ed. P. D. Singh (Dordrecht: Kluwer), 281
Rubin, R. H., Simpson, J. P., Hass, M. R., & Erickson, E. F. 1991, ApJ, 374, 564
Saraph, H. E., & Tully, J. A. 1994, A&AS, 107, 29
Seaton, M.J., Zeippen, C. J., Tully, J. A., Pradhan, A. K., Mendoza, C., Hibbert, A., & Berrington, K. A. 1992, Rev. Mexicana Astron. Astrofis., 23, 19
Snow, T. P., & Witt, A. N. 1996, ApJ, 468, L65
Souffrin, S. 1968, ApJ, 459, L61
Spinoglio, L., & Malkan, M. A. 1992, ApJ, 399, 504
Storey, P. J., Mason, H. E., & Saraph, H. E. 1996, A&A, 309, 677
Tadhunter, C. N., Fosbury, R. A. E., De Serego Alighieri, S., Danziger, I. J., & Bland, J. 1988, MNRAS, 235, 403
Thompson, R. I. 1996, ApJ, 459, L61
Tsvetanov, Z., & Walsh, J. R. 1992, ApJ, 497, 485
Veilleux, S. 1991, ApJS, 75, 357
Verner, D. A., Ferland, G. J., Korista, K. T., & Yakovlev, D. G. 1996, ApJ, 465, 487
Voit, G. M. 1992, ApJ, 399, 495
Wilson, A. S., Braatz, J. A., Heckman, T. M., Krolik, J. H., & Miley, G. K. 1993, ApJ, 419, L61
Zanstra, H. 1931, Publ. Dom. Astrophys. Obs. Victoria, 4, 209
Zhang, H. L., Graziani, M., & Pradhan, A. K. 1994, A&A, 283, 319